
Article:
Sadeghpour, A orcid.org/0000-0002-0475-7858, Ladd Parada, M orcid.org/0000-0003-1355-649X, Vieira, J et al. (2 more authors) (2018) Global Small-Angle X-ray Scattering Data Analysis of Triacylglycerols in the Molten State (Part I). Journal of Physical Chemistry B, 122 (45). pp. 10320-10329. ISSN 1520-6106

https://doi.org/10.1021/acs.jpcb.8b06704

Global Small-Angle X-ray Scattering Data Analysis of Triacylglycerols in the Molten State (Part I)

Amin Sadeghpour[1,2+], Marjorie Ladd Parada[1+], Josélio Vieira[3], Megan Povey[1] and Michael Rappolt[1]*

[1]School of Food Science and Nutrition, University of Leeds, LS2 9 JT, Leeds, U.K.

[2]Department of Materials Meet Life, Empa, Swiss Federal Laboratories for Materials Science and Technology, St. Gallen, Switzerland

[3]Nestlé, Product Technology Centre, York, U.K.

*Corresponding author: Michael Rappolt, School of Food Science and Nutrition, University of Leeds, LS2 9 JT, Leeds, U.K., e-mail: M.Rappolt@leeds.ac.uk, Tel: +44 (0)113 3431931.

[+] These authors contributed equally to the paper.

ABSTRACT

The study of triacylglycerols (TAGs) in their molten state is of fundamental importance for a deeper understanding of TAG-crystallization processes, being highly relevant for both, manufacturing and medical applications. Whilst different models have been proposed to explain the nanostructured nature of the fluid state of TAGs, none of them are fully satisfactory. In this paper, we propose a new model consisting of positionally uncorrelated lamellar TAG-assemblies embedded in an isotropic medium, that assist as pre-nucleating structures. This model was validated by applying a novel global fitting method, resulting in excellent agreement with the small angle X-ray scattering data. Deeper analysis of the scattering patterns at different temperatures, both in cooling and heating direction, allowed us further to detect crystalline traces of TAGs even after heating to 40 °C, and record on cooling the onset of crystallization at 30-25 °C. The application of the presented novel model not only explains the outstandingly structured fluid of molten TAGs, but also lays the basis for analyzing first crystallization steps in greater detail, which is outlined in our follow-up paper 'Global Small-Angle X-ray Scattering Data Analysis of Triacylglycerols in the α-Phase (Part II)'.

INTRODUCTION

Triacylglycerols (TAGs) are one of the main components of vegetable fats, and consist of three fatty acids (FAs) esterified to a glycerol backbone. In cocoa butter (CB), the source used in this study, the majority of TAGs are comprised of long FA chains (C16 to C18), most commonly palmitic (P), and stearic (S) in positions sn-1 and/or sn-3, and oleic (O) in position sn-2 and are commonly known as symmetric TAGs.[1] The food industry's central interest in TAGs relates to their functional properties which underpin the attractiveness of chocolate to consumers. Understanding the relation between TAG structure and function helps advance food formulations and related food processing techniques such as the optimization of chocolate tempering.[2] To make progress in confectionary research, links between molecular structure and physical properties of TAGs need to be understood in greater detail.[3-6] Furthermore, TAGs play a crucial role in some important diseases such as atherosclerosis and fatty liver disease.[7-9] However we note, that our main incentive for investigating cocoa butter's molecular structure in the molten state, lies in its relevance for the confectionary industry. Moreover, by analyzing a classical TAG-mixture this does lay the basis for future systematic studies on pure TAG samples, i.e. when following up more specialized questions such as the influence of chain-length and saturation to mention a few.

The first X-ray diffraction experiments on TAGs were carried out by the pioneers Clarkson and Malkin in 1934, who were among the first to analyze polymorphism of TAGs.[10] TAG polymorphism has since been widely studied, applying various methods[11-14] such as microscopy,[15-18] infrared and Raman spectroscopy,[19-23] nuclear magnetic resonance,[24-31] differential scanning calorimetry,[4, 17, 32-38] ultrasound measurements,[39-44] X-ray and neutron scattering methods[28, 45-59] and computer simulations.[59, 60] We note, that TAGs – although overall non-polar molecules – possess a slight amphiphilic character, for the glycerol backbone is moderately hydrophilic due to the partial charges of both the oxygen and carbon atoms of the ester bond, whilst the acyl chains are completely hydrophobic.[61] Therefore, they undergo aggregation into ordered structures with repeat distances in the order of few nanometers. Studies have shown the formation of amorphous/semi-crystalline states by TAGs in the liquid state,[62-69] while highly ordered crystalline structures are observed in the solid state (commonly named in the order of increasing packing density as α-, β'- and β-polymorphs).[6] In this study, however, we will concentrate on the molten state of TAGs, before we revisit, in a second part, the structure and formation of the α-polymorph coexisting with a high amount of molten TAGs.

For TAGs in the liquid state, small angle X-ray and neutron scattering (SAXS, SANS) measurements display a broad diffuse peak at around 2.6 nm^{-1}, which is equivalent to a

characteristic distance of 2.4 nm.[46, 68] The position of this broad peak varies slightly among different types of TAGs depending on the chain length, chain saturation and the position of the FAs along the glycerol backbone. Other physical and environmental conditions may also influence the semi-crystalline states such as temperature, pressure, and sample history.[70] Nevertheless, a fully satisfying explanation of this observed fluid ordering phenomenon has yet to be delivered. Three main different structural models for the molten state of TAGs have been proposed, namely (i) smectic, (ii) nematic and (iii) discotic arrangements of TAGs.[68, 71, 72]

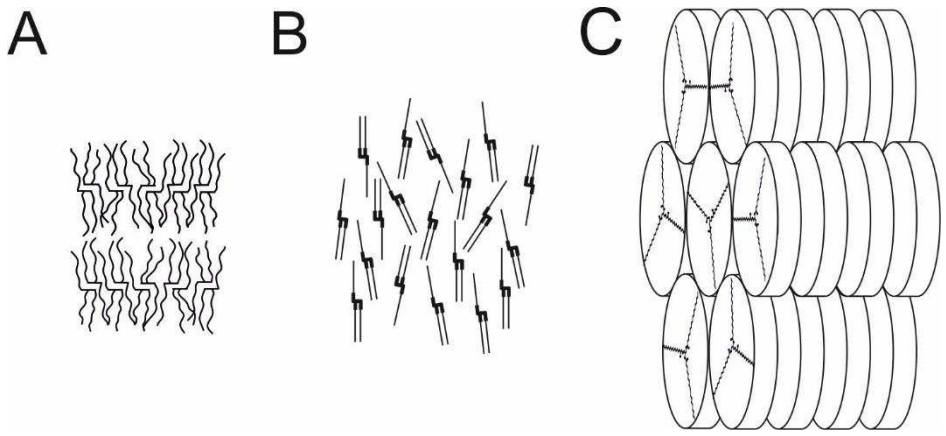

Figure 1. (A) Smectic,[73] (B) nematic[69] and (C) discotic[63] arrangement of TAGs in the molten state. The proposed models base on qualitative interpretation of X-ray and neutron scattering data.[68, 71, 72] The Y-conformation of a single TAG in the discotic phase is also shown in panel C.

In the smectic model proposed by Larsson,[71] h-conformed TAGs are believed to form a lamellar liquid-crystalline phase with very loosely stacked bilayers, i.e. with a complete lack a long-range order (Figure 1A). This means, each lamella has roughly the thickness of two fatty acid chain length – also known as "2L layer" arrangement – and all the chains within a lamella layer align in one direction only. Importantly, Larsson described a system with stacked layers, but the stacks being highly disordered thus accounting for the absence of diffraction peaks in the recorded X-ray and neutron data.

Cebula et al.[68] criticized the well-defined lamellar structure proposed by Larsson. Based on neutron diffraction evidence from trilaurin whose glycerol hydrogens were replaced with deuterium increasing the neutron scattering from the glycerol backbone, they argued that such smectic structure is unlikely to exist, otherwise, sharper and more dominant reflections should be observed in the scattering pattern arising from both, the given long- and short-spacings, respectively. Consequently, they proposed a nematic model for TAG arrangement in the liquid state to reflect the neutron data more satisfactorily (Figure 1B). They further explicate that the observed reduction of the characteristic lamellar repeat distances (comparing neutron data from liquid and solid TAG phases) is due to both, the interdigitation of the FAs given in the nematic arrangement, and the effective shortening of FA chains above the melting point (arising from

the given *trans-gauche* conformers of each chain).[74] The main weakness of the nematic model, as pointed out later by Larsson,[67] lies in the general requirement for the existence of stiff, rod-like molecules for its formation, which is not the case for TAGs displaying a high chain mobility above the melting point. Secondly, given the vast number of liquid crystalline lipid structures published, it seems unlikely that a nematic arrangement of lipids has never been observed beforehand. Noteworthy, despite the differences between the proposed models by Larsson and Cebula, they both suggest an h-conformation of TAGs; however, based upon molecular shape arguments and computer simulation, Corkery et al.[72] argued that the chains of a single TAG molecule can splay into an entropically driven Y-conformer in the melt, which could lead to the formation of a discotic arrangement of TAGs (Figure 1C).

In the discotic model, these Y-conformers exhibit time-averaged disc-like shapes and are assumed to assemble into flexible cylindrical rods or columns via interdigitated stacking of the TAGs. In turn, these TAG-stacked rods are believed to loosely pack (also with interdigitation) into time-averaged disordered hexagonal mesophases.[63] While this model can be argued being in agreement with the published scattering data, it remains unsatisfactory that this discotic lipid mesophase can remain stable, as throughout the Y-conformers all there is to keep this complexly structured assembly intact are only reduced, non-aligned van der Waals forces.

Interestingly, Tascini et al.[59] predicted recently from their molecular dynamics simulation studies on the fluid state of sebum triacylglycerol (note, all three FAs are 16:1 with a double bond at position 6), a clustering of TAGs' glycerol backbones leading to a single percolated network. This clustering of TAGs headgroups – as we will demonstrate in the following - is confirmed also in our experimental modelling of TAGs in the molten state, but nevertheless, we do return in our study to the idea of planar TAG clusters, which seems the most appealing approach, since the nascent solid polymorphs of TAGs are of lamellar nature. We note, however, based on this recent simulation data,[59] that we are discussing the possible dimensionality of the forming clusters in the molten state with great care (1D-wormlike *versus* 2D layered clusters). Secondly, in contrast to the Larsson's model, we are <u>not</u> considering any lamellar stacking, but suggest two differently assembled TAG-layered models and test their validity with experimental SAXS data. Furthermore, we are treating these lamellar assemblies to be positionally uncorrelated, i.e., being embedded in an isotropic medium of molten TAGs.

Eighteen years of experience with the modelling of planar lipid mesophases[75-77] enabled us to develop a similar global fitting procedure for TAGs in the molten state. This new model allows a high resolution portrayal of the local molecular organization of mixed TAGs in the

fluid phase over a wide temperature range and is also in excellent agreement with the given SAXS data without the need for highly speculative interpretations.

MATERIALS AND METHODS

Sample Preparation

West African cocoa butter (CB) provided by Nestlé, PTC, York, U.K. was used without additional refining. Two 1.5mm quartz disposable capillaries were filled with molten CB (at 50 °C) and sealed with wax and epoxy glue. The samples were then allowed to cool at room temperature and kept under this condition for at least one week to ensure the presence of the β-V polymorph. Its formation was confirmed through preliminary small- and wide-angle X-ray (SAXS/WAXS) measurements taken with an exposure time of 5 minutes. While there are many other solid polymorphs known for TAGs[46], we note, that the β-V polymorph is the most relevant phase in chocolate production, and hence was chosen as experimental starting point.

X-ray Scattering Measurements

Both, SAXS and WAXS experiments were performed with the SAXSpace instrument (Anton Paar GmbH, Graz, Austria) equipped with a Cu-anode that operates at 40 kV and 50 mA (λ = 0.154 nm). The instrument is equipped with a temperature-controlled stage (TCStage 150, Anton Paar, Graz, Austria) working in a range from -30 to 150 °C (precision 0.1 °C).

The scattering vector modulus, q, was calibrated with silver-behenate. The sample-detector distance used for the SAXS measurements was 317 mm and for the simultaneous SAXS and WAXS measurements 130 mm. We note that the latter set-up was only relevant for ensuring the samples to have formed the stable β-V polymorph beforehand ($0.1\ \text{nm}^{-1} \leq q \leq 18\ \text{nm}^{-1}$ with $q = (4\pi/\lambda)\sin(\theta)$, where 2θ is the scattering angle). More significantly, the SAXS-setup covered the angular scattering range of $0.07\ \text{nm}^{-1} \leq q \leq 8\ \text{nm}^{-1}$. The 1D scattering patterns were recorded with a Mythen micro-strip X-ray detector (Dectris Ltd, Baden, Switzerland). Note all simulated model functions were smeared using the experimentally determined length-profile of the X-ray beam (20 mm width) of the SAXSpace camera. More specific details on the X-ray scattering set-up and the standard data reduction protocols can be found in reference.[78]

Once the presence of the β-V form was confirmed, the sample was allowed to equilibrate at 20 °C in the sample stage of the SAXSpace instrument, followed by a heating protocol based on the methodology of Da Silva and Rousseau[21]. The sample was heated from 20 °C to 35 °C

in 5 °C degrees steps, followed by 37 °C (body temperature), 40 °C, and subsequently heated to 110 °C in steps of 10 °C. The sample was then cooled down to 20 °C, following a reversed protocol in cooling direction. At each programmed temperature the sample was equilibrated for 10 minutes and an exposure time of 20 minutes was used.

Analysis of the Broad Scattering Contribution from TAGs in the Molten State

The temperature-resolved analysis of the broad scattering maxima of the SAXS patterns was firstly carried out applying a Gaussian distribution using Origin Pro 9.1®

$$I(q) = y_0 + \frac{A}{w\sqrt{\left(\frac{\pi}{2}\right)}} \cdot \exp\left(-2\left((q - q_c)/w\right)^2\right) \quad (1)$$

where y_0 is the offset, $w = 2\sigma$ is the width of the distribution, A is the area under the bell-shaped curve and q_c marks the center of the distribution. From the latter parameter, we can deduce a characteristic distance of the semi-ordered TAGs in the molten state

$$D = 2\pi/q_c \quad (2)$$

The full width half maximum (FWHM) in reciprocal space is given by

$$FWHM(q) = w\sqrt{\ln(4)}, \quad (3)$$

from which the *FWHM(z)* in real space can be calculated (see SI) by

$$FWHM(z) = \frac{2\pi\, FWHM(q)}{{q_c}^2 - (FWHM(q)/2)^2} \quad (4)$$

We note that the *FWHM(z)* gives a only qualitative measure of the size distribution of the characteristic distance, *D*, of the semi-ordered TAGs in the molten state.

Global SAXS Data Analysis Applying Novel Lamellar TAG Assembly Models

To take a closer look at the structuring of TAGs in the fluid phase, we have applied a tailored global analysis approach introduced successfully more than 17 years ago for the global analysis of X-ray and neutron scattering from phospholipid bilayer structures.[75-77] The scattering intensity of aligned lamellar stacks can be described by

$$I(q) = \frac{S(q)\,|F(q)^2|}{q^2} \quad (5)$$

in which q is the scattering vector modulus, $F(q)$ is the form factor (arising from the lamellar motif) and $S(q)$ is the structure factor (arising from the stacking order). In the models for TAGs in the molten state proposed in this study, we assume the absence of positionally correlated

layers. In other words, while we consider the *formation of lamellar TAG assemblies*, these lamellae are not assumed to align in stacks, but rather, are embedded in an isotropic medium of molten TAGs (Figure 2A). Therefore, we omit the structure factor contribution and the scattering intensity can be simplified[79] to

$$I(q) = \frac{|F(q)^2|}{q^2} \tag{6}$$

For a flat layered structure, we can obtain the form factor *F(q)* from the one-dimensional Fourier transform (FT) of the electron density profile across the depth of the layer that we model as a summation various Gaussian peaks (one-dimensional) each representing a particular molecular moiety or region.[77, 80] The form factor can then be written for centrosymmetric profiles (*F'(q)*) in the in general form[81]

$$F'(q) = q^{-1} \sum_{k=1}^{n} \rho_k \sigma_k \exp\left(-\frac{q^2 \sigma_k^2}{2}\right) \cos(q z_k), \tag{7}$$

where ρ_k denotes the amplitude of the Gaussian, σ_k the width and z_k its position. Note, a factor of q^{-1} must be added to relate the one-dimensional FT correctly to the three-dimensional spherical metrics of reciprocal space (for further discussion see details in the SI). Above in Eq. 6 this was accomplished by applying a Lorentz correction of q^{-2}.[79] We note, correcting for spherical geometry, the final scattering intensities does decay by q^{-2}, indicating the planar nature of scattering objects, which are randomly oriented in all directions.

In our first model, we constructed the electron density distribution as a linear combination of two Gaussian functions. This simple 2-Gaussian electron density model is constructed according to equation

$$\rho_{II}(z) = exp\left(-\frac{(z)^2}{2\sigma_G}\right) - \rho_r \sum_{j=1,-1} exp\left(-\frac{(z - j z_C)^2}{2\sigma_C}\right), \tag{8}$$

which the first term describes the electron density distribution of the glycerol backbone at the center of the layered TAG assembly (zero position along z-axis) with distribution breadth of σ_G. The second term represents the electron density distribution around the lipid hydrocarbon methyl groups (CH_3) positioned at either side, z_{CH_3} and -z_{CH_3} with the distribution breadth given by σ_C. The amplitude $\rho_r = |\rho_C/\rho_G|$ denotes the relative electron density contrast of CH_3 groups normalized with glycerol backbone electron density, ρ_G. Please note, that this normalization pays tribute to the fact that the electron density contrasts ρ_C and ρ_G are not linear independent variables, thus allowing us to define $\rho_G := 1$. Finally, the squared Fourier transform for the above electron density function can be calculated by[76, 81]

$$F_{II}(q)^2 = 2\pi \left[\sigma_G \exp\left(-\frac{{\sigma_G}^2 q^2}{2}\right) - 2\rho_r \sigma_C \exp\left(-\frac{{\sigma_C}^2 q^2}{2}\right)\cos(qz_C)\right]^2 \quad (9)$$

Nevertheless, as will be shown in the results section, the 2-Gaussian model does not fit the SAXS data perfectly. Thus, we designed an extended model using 3-Gaussian distributions to construct the electron density distribution considering a loose attachment of an additional shell of TAGs to the central core of our previous model (Eq. 8). This electron density profile is formulated by

$$\rho_{III}(z) = exp\left(-\frac{z^2}{2\sigma_G}\right) - \rho_r \sum_{j=1,-1} exp\left(-\frac{(z-jz_C)^2}{2\sigma_C}\right) + |\rho_{shell}| \sum_{j=1,-1} exp\left(-\frac{(z-jz_{shell})^2}{2\sigma_{shell}}\right) \quad (10)$$

in which the $|\rho_{shell}|$ is the relative electron density contrast of the lower concentrated glycerol regions of the second TAGs layer, again normalized with glycerol backbone electron density, ρ_G and $\pm z_{shell}$ represents its position along z-axis (Figure 1B). Similarly, the Fourier transform leads to

$$F_{III}(q)^2 = 2\pi \left[\begin{array}{c} \sigma_G \exp\left(-\frac{{\sigma_G}^2 q^2}{2}\right) - 2\rho_r \sigma_C \exp\left(-\frac{{\sigma_C}^2 q^2}{2}\right)\cos(qz_C) \\ +2|\rho_{shell}|\, \sigma_{shell} \exp\left(-\frac{{\sigma_{shell}}^2 q^2}{2}\right)\cos(qz_{shell}) \end{array}\right]^2 \quad (11)$$

Finally, the experimental intensity data (Eq. 6) were globally fitted by using a Particle Swarm Optimization (PSO) method[19] to avoid local minima fitting solutions.

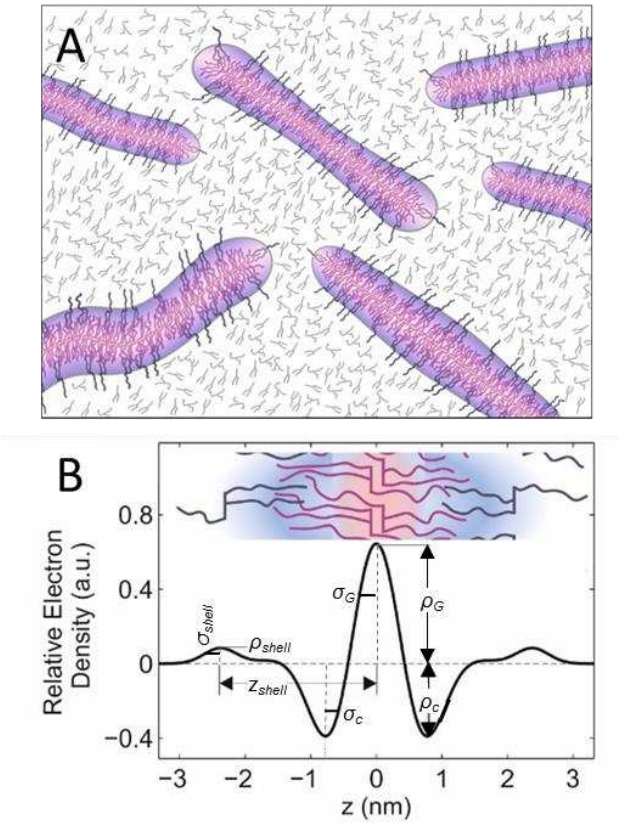

Figure 2. Lamellar TAG assembly model. (A) Schematic sectional representation of the lamellar TAG assembly model. The TAGs back-to-back assemblies are treated as 2D-lamellar double layers (red-purple) with a loosely attached outer layer of TAGs (black). Note, that the lateral extension of the assemblies are assumed to be practically infinite, when compared to the thickness of the lamellae. Non-assembled TAGs are shown in light grey. (B) Electron density profile modelled with three Gaussian distributions identifying (i) the high density glycerol backbone region (centered at the origin), (ii) the low density hydrocarbon chain regions (methyl group rich) and (iii) low density glycerol backbone regions (loosely attached second layer).

RESULTS AND DISCUSSION

Overall Size and Ordering Trends as a Function of Temperature

In the liquid state of CB, a broad scattering distribution around 2.3 nm^{-1} was recorded over a wide temperature range, i.e. from 40 °C up to 110 °C (Figure 3A). On cooling, this broad peak roughly displays the same position and width as on heating, but the fluid phase remains stable also during undercooling down to 20 °C. This broad diffuse scattering, at first glance, confirms the existence of a semi-ordered structure. A detailed analysis of the scattering profiles over the examined temperature range reveals that the sharpness of the peak slightly increases by reducing the temperature, thus demonstrating that more ordered structures are formed when cooling. These observations agree with the general law of temperature driven entropy changes.

However, for providing a quantitative picture about molecular organization, we fitted all SAXS patterns with a Gaussian distribution.

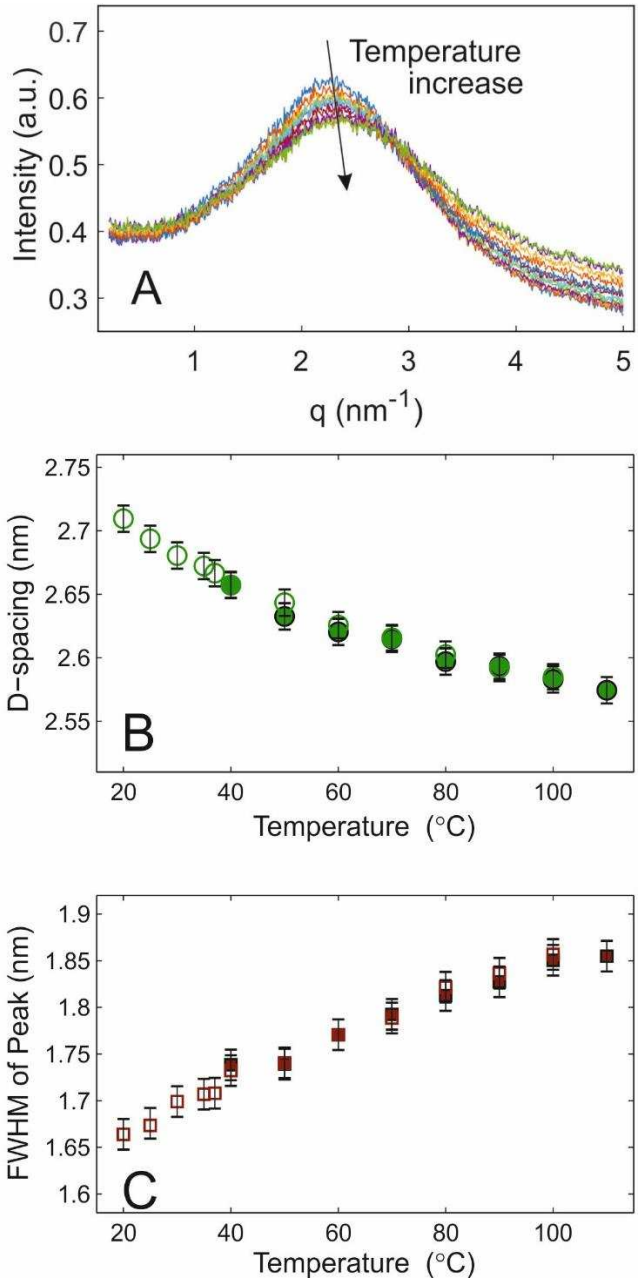

Figure 3. Standard SAXS analysis. (A) SAXS-data taken in a temperature range from 40 to 110 °C. (B) Characteristic distance, *D(z)* and (C) *FWHM(z)* of the diffuse scattering peaks as a function of temperature. The closed and open symbols represent the data extracted from heating and cooling cycles, respectively.

The temperature induced variation on the position of peak in the SAXS profiles can be related to the changes in clusters' dimension. The peak position provides a characteristic length, *D(z)*, of the assemblies in the fluid state (Figure 3B), whilst the *FWHM* in real space provides an idea of the dispersion of the characteristic extension, i.e. the larger the *FWHM*, the larger the variation of the *D*-spacing (Figure 3C; note the *FWHM(z)* is calculated to according to Eq. 4).

From this standard data analysis, it can be seen that characteristic length of the TAG assemblies in the fluid state decreases monotonically with increasing temperature (Figure 3B) in agreement with Lin.[82] We assume that during the heating process this is related to the increasing number of *gauche* conformers per hydrocarbon chain. Since this induced chain disorder leads to an overall shortening of the chains in TAG molecules, the reduction in *D(z)* makes sense, if related to the effective chain length of the TAGs. Regarding the *FWHM(z)* (Figure 3C), as expected, its values increased alongside the temperature. This suggests that as temperature increases, the mobility of the TAGs also increases, resulting in a wider spread of characteristic length, *D(z)*.

Novel Lamellar TAG Assembly Models for the Fluid State

In contrast to diffraction data, a global detailed analysis of the broad diffuse scattering from TAGs in the molten state requires the application of indirect Fourier transformation methods. In this study, we report on such quantitative SAXS data analysis for TAGs for the first time. In our novel fitting procedure, we applied a global analysis approach[77, 79] to refine the electron density profiles (EDP) of TAG aggregates parallel to the membrane normal. In this approach, a multi-Gaussian function representing the EDP is applied, leaving their position, height and width as free fitting parameters (see methods section). These real-space functions (Eq. 8 and 10) are Fourier transformed, and then used to fit the experimental scattering curves (Eq. 9 and 11; Figure 4).

The simplest lamellar TAG assembly model used comprises two Gaussian distributions, one at the center representing the region of back-to-back arranged glycerol backbones (high electron density region) and the second Gaussian representing the region of an increased methylene-group density (CH_3) on either side from the center (Figure 4B, 2-G core cluster model). Although the fits based on this 2-G model are acceptable (Figure 4A, dashed line), the sharpness of the scattering lobe and the low *q*-scattering intensities are not satisfactorily reproduced. Moreover, the position of the methylene group regions seems to be too close to the center (at ± 0.9 nm), when compared to the chain length of the TAGs (mainly C18:1, C18 and C16) in the molten state. We note that the expected chain length of oleic and oleic/palmitic acid mixtures is in the order of 1.3 nm.[83, 84] Hence, we decided to improve the model further and include a second layer of loosely attached TAGs (Figure 2; Figure 4B, right hand side).

Like the previous 2-G model, the first function represents the central glycerol backbone region, and the second Gaussian denotes the region of an increased methyl-group density. In addition, a third Gaussian is considered, which reflects the position of the glycerol backbones

relative to the loosely attached TAGs in the outer shell of the cluster (Figure 4B, 3-G core-shell cluster model). The relative height of the third Gaussian can be tuned up/down to strengthen/weaken the electron density contrast arising from the outer shell of the cluster.

Optimization of the data led to a perfect SAXS fit, as seen in Figure 4A (solid line), for the scattering profile recorded at 20 ºC (after cooling). A detailed look into the EDP revealed that the TAG overall cluster thickness is of approximately 4.74 nm (backbone-to-backbone distance), leading to a double layer (2L) thickness of 2.37 nm on either side of the center. With expected chain lengths in the molten state of about 1.3 nm (see above), this means the second layer of loosely attached TAGs is most probably slightly interdigitating with TAGs of the core double layer in the order of 0.1-0.2 nm (Figure 2B and on the right hand side of Figure 4B).

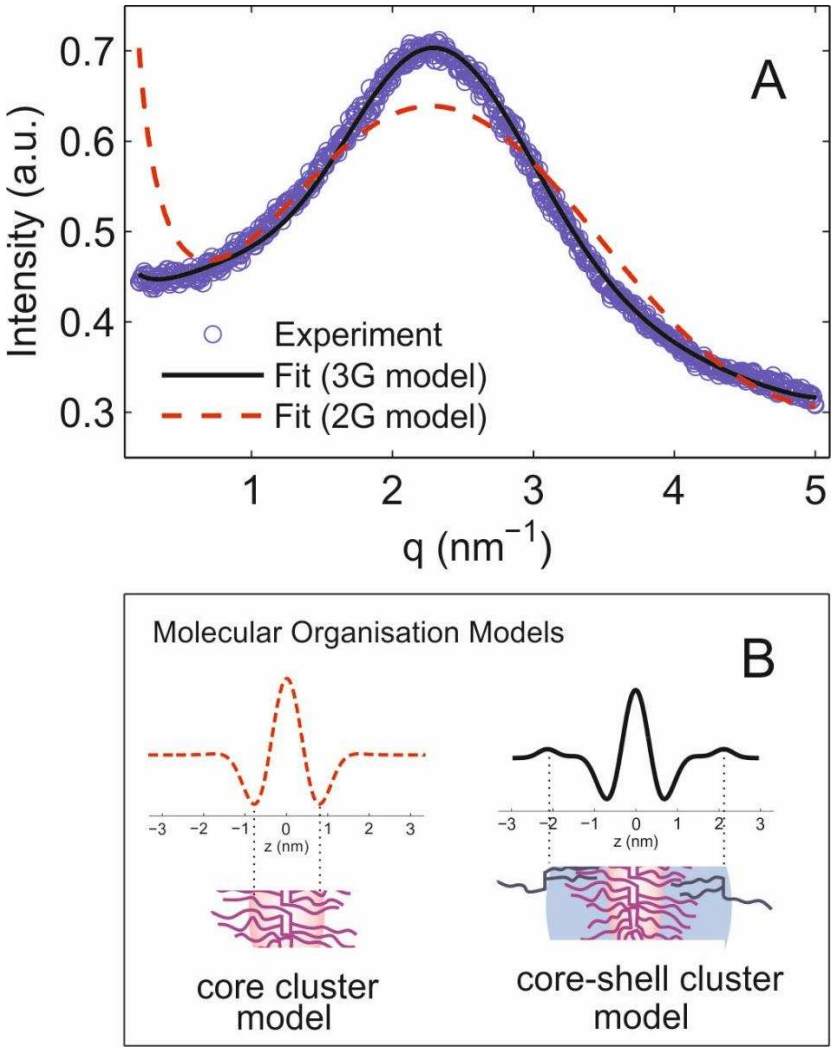

Figure 4. (A) Experimental SAXS pattern from molten TAGs at 20 ºC (blue circles) and the simulated scattering profile with 2-Gaussian (dashed line and left hand diagram in panel B and 3-Gaussian form factor model (solid line and right hand diagram in panel B). (B) The electron density distribution curves are represented together with the corresponding molecular cluster model schemes. Note, the complete data-set fittings are presented in Figure S1 in the supplementary information.

Inner Core and Overall Cluster Size Dimensions as a Function of Temperature

From the 3-G model two main extensions perpendicular to the lamellar TAG assemblies were analyzed in more detail as a function of temperature, namely one reflecting the cluster core thickness, and the second extension being correlated to the overall thickness of the cluster, i.e. including the second layer of loosely attached TAGs (Figure A). The variations in core and overall cluster thickness are in the order of a few tens of nanometers as can be judged from the scatter of the data points in Figure 5B and C. The core thickness is reduced with increasing temperature, from 1.25 nm, at 20 ºC, to 1.18 nm, at 110 ºC. Note that these values are now larger than the previously calculated thicknesses using the 2-G model, and in good agreement with literature values.[83, 84] Similarly, the overall cluster dimension (the core plus the shell

thicknesses) varies with temperature. We determined a cluster dimension of 4.67 nm, at 110 ºC, which increases to 4.76 nm once 20 ºC were reached. While these trends in lamellar cluster thicknesses are well understood assuming an increasing chain disorder as a function of temperature (increased number of *gauche* conformers per chain),[74] the overall changes are small, showing that the chain disorder within the lamellar assemblies does not vary strongly as a function of temperature.

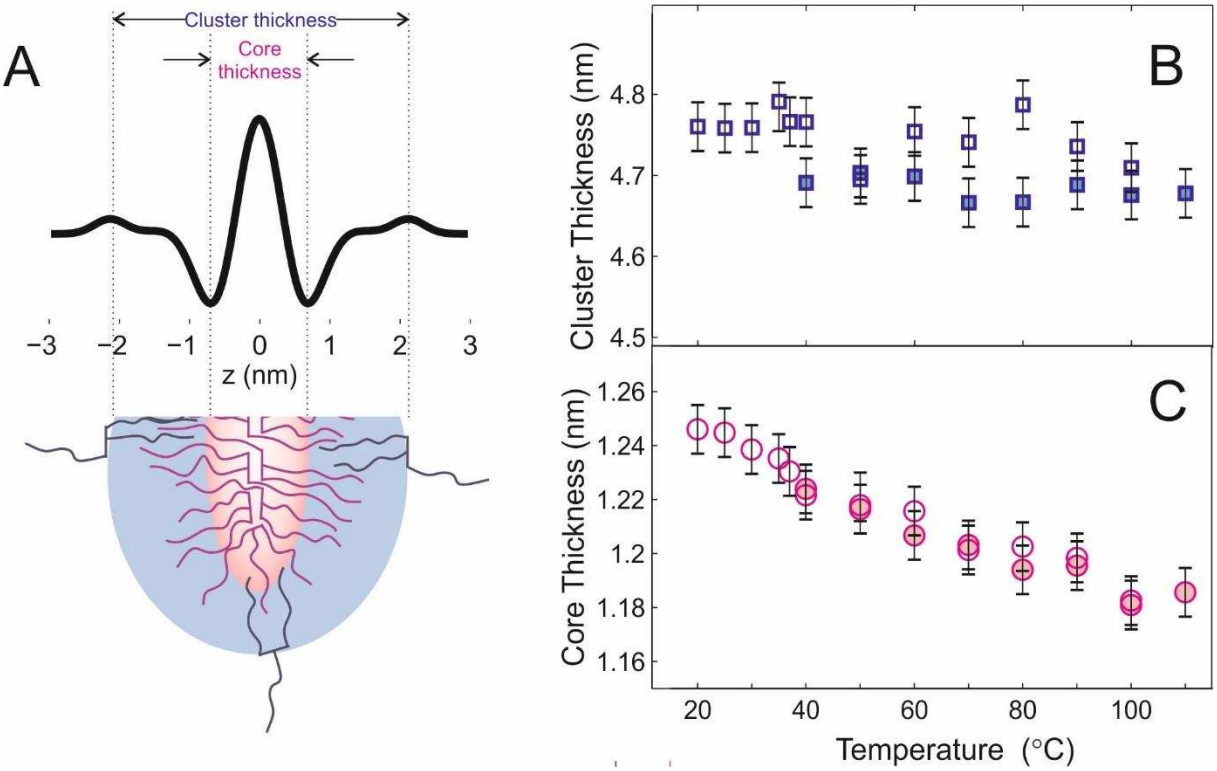

Figure 5. The core-shell cluster dimensions extracted from the electron density profiles (EDPs in A) calculated from the SAXS data. Note, the standard deviation of the cluster thickness is ±0.06 nm (B) and the standard deviation of the core thickness is ±0.03 nm (C). That is, cluster thicknesses do show a slight hysteresis effect, while within in error the core thickness does not. The closed and open symbols represent the data extracted from heating and cooling cycles, respectively.

Fine Analysis of the Temperature Dependence of the Second TAG Layer

Fine analysis of the scattering profiles over the heating and cooling cycle shows that the relative height of the third Gaussian in the EDPs decreases with temperature (Figure 6). This height is directly related to the electron density contrast of the glycerol backbones of the second TAG layer. The more TAGs attach to the outer shell, the higher this contrast emerges in the EDP; accordingly, the scattering profile displays a sharper, less broad, diffuse peak at ca. 2.4 nm^{-1} (Figure 3C). To quantitatively describe the attachment behavior of TAGs in the shell, we concentrate on the fitting parameter $|\rho_{shell}|$, which reflects the relative electron

density contrast of the lower concentrated glycerol regions of the second TAG layer. Since $|\rho_{shell}|$ is normalized to the electron density contrast of the glycerol backbone from the center of the cluster, its value corresponds to the relative percentage of loosely attached TAGs in the shell. We note that a full occupational state in the second TAG layer is reached with $|\rho_{shell}|$ = 50 %, as the centered TAGs are arranged in a back-to-back fashion, while the shell exhibits just one layer of TAGs. Having said this, we can estimate that just above the melting point (37 °C), roughly 14% of the second layer is occupied by TAGs in an ordered fashion, which diminishes to 10% at 110 °C. Upon cooling the sample, the fraction of occupancy in the second layer increases up to roughly 17%.

Interestingly, we also observe a small, but significant hysteresis effect. For instance at 40 °C, during heating $|\rho_{shell}|$ is above 7% (TAG occupancy in the outer shell >14%), whilst in the cooling scan, it is less than 7% (TAG occupancy in the outer shell <14%). This is expected as prior to starting the heating scan the sample was in the solid state (β-V polymorph), thus, the TAG occupancy is initially complete, and then slowly decays with increasing temperature. In contrast, on cooling, the liquid to solid transition is not only driven by thermodynamics, but more importantly governed by kinetic interactions that delay the assembly process of the shell, and hence the onset of crystallization.[85-87] Nevertheless, what is particularly noteworthy is that the hysteresis can also be observed at temperatures more than 40 °C above the melting point of CB (37 °C[51]). If we consider that the obtained hysteresis between heating and cooling ramps is directly related to differences in occupation level, i.e. structuring or degree of ordering in the molecules, then it is possible to assume that some level of structuring is retained up to approximately 80 °C and is only “erased” on heating to higher temperatures. Given that this temperature is close to the melting point of the β-form of tristearin, the previous would support the proposed order of crystallization in CB, where the first TAGs to crystallize would be the fully saturated ones.[88-92]

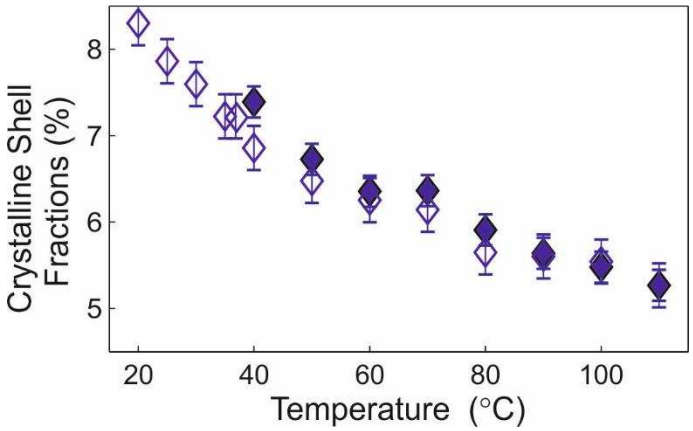

Figure 6. The variation of relative electron density contrast of the lower concentrated glycerol backbone regions of the second TAGs layer. The relative electron contrast values of the shell are given in percent with respect to the glycerol backbone contrast of the core. The closed symbols represent the data obtained during heating cycle and the open symbols demonstrate the ones extracted over the cooling cycle.

Crystalline Traces in the Fluid Phase of TAGs

Despite the successful simulation of scattering data from the molten TAGs mixture, we observed very weak traces of diffraction, specifically at lower temperatures. These weak traces became more evident on subtraction of the simulated data from the experimental one. In Figure 7, the residual scattering data with respect to our fitted data are displayed in a color-contour plot for the entire temperature range for the heating and cooling scans. This residual scattering is more intense at the beginning of the heating cycle, and covers the range related to both 3L (q = 0.9 nm^{-1}), and 2L (q = 1.25 nm^{-1}) structures, which can be associated with some remaining lamellar structures from the crystalline phase (β-V). However, above 50 °C these residues decrease substantially, until at 110 °C no significant crystalline structures remain. Contrastingly, in the cooling scan, it is not until the undercooling regime below 30 °C that more intense residues are noticeable. In this case, these residues are found only at approximately 1.2 nm^{-1}, which might indicate the onset of crystallization of the higher melting TAG species of CB, as proposed by previous workers.[88, 92] It is tempting to assume that the proposed pre-nucleating structures (Fig. 2 and 5) act as templates for crystallization, similarly to monoacylglycerols and surfactants when mixed with fats.[93-99]

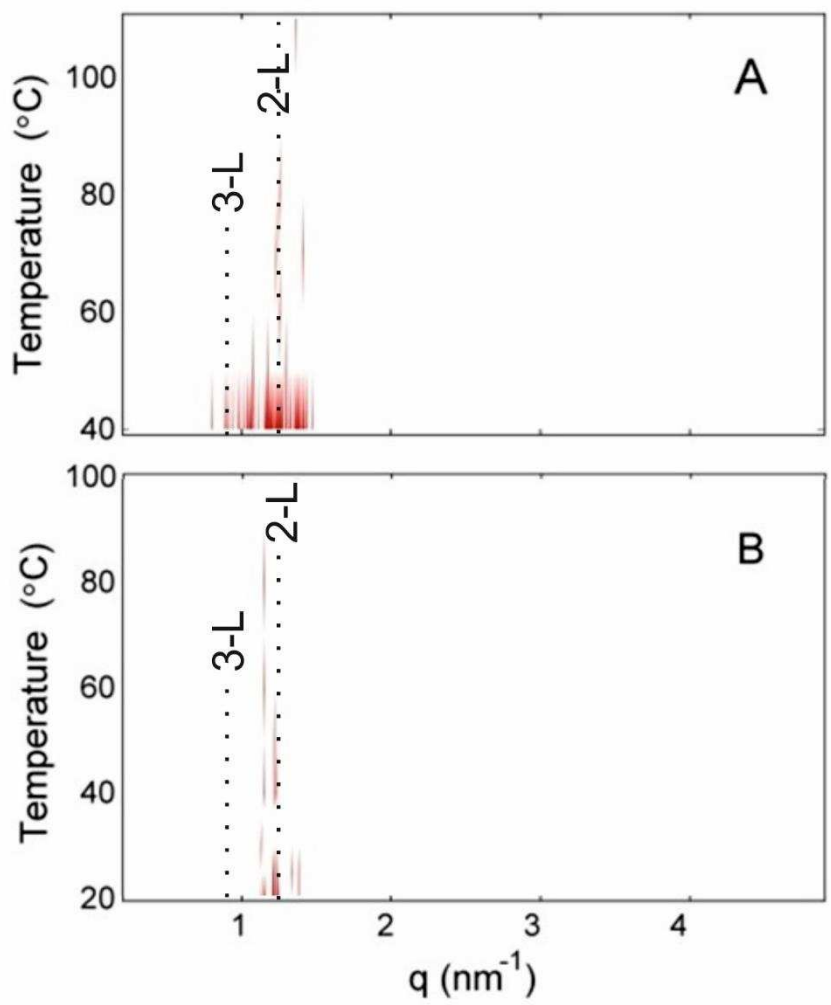

Figure 7. The residual scattering (theoretical scattering intensity subtracted from experimental scattering intensity) represented during A) heating and B) cooling of TAGs. A darker shade of red represents a stronger intensity of the residues. A darker shade of red indicates an increased amount and intensity of residual scattering. Dotted lines indicate expected diffraction peaks arising from for 2-L and 3-L stacking, respectively.

In summary, the residual scattering on heating indicates that CB is not fully molten at 37 °C, as is frequently assumed in literature.[54] In addition, on cooling, traces of crystallized TAGs can be associated with the formation of crystal nuclei with 2L structures that are only evident below 25 °C after an equilibration time of 10 minutes. Based on our nanostructural findings, it is plausible that these very few nuclei will start to grow in number and size once the second TAG-layer in our pre-nucleating 3-G model is fully occupied (see Figure 2 and 6). Note, once intact two TAG double-layers (2L) are completed, solidification of this 4L-cluster would be energetically favorable, driven by the maximized van der Waals interaction between neighboring FA chains. In turn, these smallest thinkable solid 4L-nuclei, could subsequently trigger an epitaxial lamellar growth, leading to the formation of solid crystal polymorphs.[6, 73, 100, 101]

Conformational and Dimensionality Considerations of Clustered TAGs

Our proposed model of clustering TAGs in the fluid phase of cocoa butter (Fig. 2) combines structural elements of all three previously proposed smectic-, nematic- and discotic-based models[68, 71, 72] (Fig. 1). The 'back to back' arrangement of TAGs in the core displays a smectic motif, while the second layer of TAGs is attached to the core in a loose nematic fashion. Third, the strongly curved edges of the clusters are expected to accommodate mainly 'Y-conformer' TAGs, just as proposed in the discotic model.[72] Interestingly, the latest simulation data on entirely unsaturated TAGs predict a distribution a mix of four different conformers due to the high mobility of the chains above their melting point.[59] The main conformer is the 'tuning fork' (39%), where chains at the sn-1 and sn-3 position point in the same direction, whilst the sn-2 fatty acid points in the opposite direction. The second largest population (28%) concerns the 'Y-conformation', which Tascini et al.[59] call the 'propeller conformation'. They further propose the presence of two other minor populations, a 'chair' or 'h-conformer' (18%) and a 'trident conformation' (16%), in which all three FAs point in the same direction. We note, that this simulated conformer distribution agrees well with our proposed TAG cluster model, assuming the edges to be rich in 'Y-conformers' and the planar regions to be mainly populated by 'tuning fork', 'chair' and 'trident conformers'.

Lastly, we shall discuss the lateral extension of the proposed cluster formation model. It is important to note, that the X-ray scattering patterns are mainly governed by the proposed EDP contrast perpendicular to the plane normal, and the SAXS analysis is less sensitive to the lateral extension of the clusters. In extremis, – keeping the same EDP-model – we cannot entirely exclude that the TAGs assemble in a wormlike fashion (see supporting information for testing 1D versus 2D lateral cluster extension, Figure S2). On the one hand, the latter scenario mimics better the predicted single percolated network as proposed by molecular dynamics simulation.[59] On the other hand, based on polarized microscopy studies,[102, 103] we remark that this single percolated network cannot explain the stochastic nature of primary nucleation within the fluid bulk phase of TAGs,[104] and secondly, it is difficult to envisage how the nascent smectic α-phase will evolve from wormlike 1D-nuclei. A possible scenario could also be that high temperature molten TAGs display more 1D-wormlike clusters, which when approaching the transition temperature start to grow also laterally, providing the structural basis for first planar nuclei.

CONCLUSION

In this study, we propose a new model for the nanostructured fluid of molten TAGs in CB. A core layer of TAGs is considered, with their glycerol backbones assembled in ‘back-to-back’ fashion, and their FA chains extending outwards. A second layer of loosely attached TAGs (7-14% occupancy) turned out to be crucial to explain satisfactorily the X-ray scattering data. We observed that the occupancy of this second layer of TAGs decreases with temperature, and likewise, as temperature drops, the level of TAGs in the shell increases. Our final hypothesis is that once this second shell is fully occupied, the crystallization of TAGs can commence.

Finally, the goodness of the obtained fits permitted to detect traces of crystallized TAGs by their subtraction from the experimental data. This allowed identifying crystalline structures even above 40 °C, on heating. Remarkably, the presence of crystalline nuclei is also observed from approximately 30-25 °C on cooling. The previous observations together with the finding of an increased occupancy of TAGs in the outer shell at lower temperatures, implies that the proposed self-assembled lamellar clusters of molten TAGs may serve as pre-nucleating structures, wherein their planar surfaces aid the lamellar epitaxial growth commonly detected in crystallizing TAGs. Nevertheless, this proposed nucleation mechanism does not exclude additional heterogeneous nucleation induced by the foreign material inherently present in vegetable fats, such as microscopic milling residues from the outer shell of CB.

AUTHOR INFORMATION

Corresponding Author

Michael Rappolt

School of Food Science and Nutrition, University of Leeds, LS2 9 JT, Leeds, U.K.

E-mail: M.Rappolt@leeds.ac.uk

Tel: +44 (0)113 3431931

Author Contributions

The manuscript was written through contributions of all authors. All authors have given approval to the final version of the manuscript. [+]These authors contributed equally.

ACKNOWLEDGMENT

The authors would like to thank Nestlé for providing the cocoa butter used in this study, as well as providing financial support for Marjorie Ladd Parada's PhD project. This work was funded by the Consejo Nacional de Ciencia y Tecnología (México) in the manner of a full scholarship for the PhD studies of Marjorie Ladd Parada.

ABBREVIATIONS

TAG, triacylglycerol; SAXS, small-angle X-ray scattering; SANS, small-angle neutron scattering; CB, cocoa butter; WAXS, wide angle X-ray scattering; EDP, electron density profile; FWHM, full width half maximum.

TABLE OF CONTENTS IMAGE

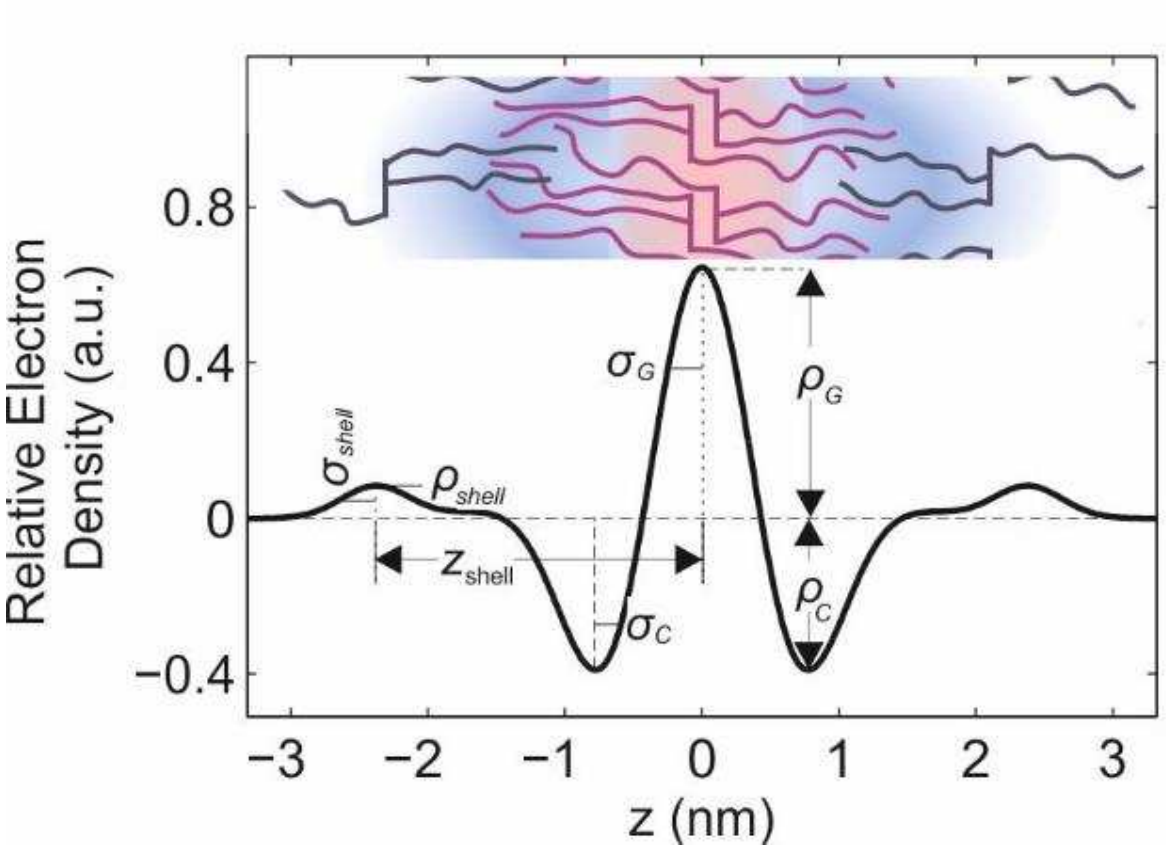

REFERENCES

1. Lipp, M.; Simoneau, C.; Ulberth, F.; Anklam, E.; Crews, C.; Brereton, P.; de Greyt, W.; Schwack, W.; Wiedmaier, C., Composition of Genuine Cocoa Butter and Cocoa Butter Equivalents. *Journal of Food Composition and Analysis* **2001,** 14, (4), 399-408.

2. Toro-Vazquez, J. F.; Dibildox-Alvarado, E.; Herrera-Coronado, V.; Charó-Alonso, M., Triacylglyceride Crystallization in Vegetable Oils: Application of Models, Measurements, and Limitations. In *Crystallization and Solidification Properties of Lipids* 1st ed.; Widlak, N.; Hartel, R.; Suresh, N., Eds. AOCS Press: Champaign, Illinois, U.S.A., 2001; pp 53-78.

3. Acevedo, N. C.; Marangoni, A. G., Characterization of the Nanoscale in Triacylglycerol Crystal Networks. *Crystal Growth & Design* **2010,** 10, (8), 3327-3333.

4. Acevedo, N. C.; Marangoni, A. G., Toward Nanoscale Engineering of Triacylglycerol Crystal Networks. *Crystal Growth & Design* **2010,** 10, (8), 3334-3339.

5. Brunello, N.; McGauley, S. E.; Marangoni, A., Mechanical properties of cocoa butter in relation to its crystallization behavior and microstructure. *LWT - Food Science and Technology* **2003,** 36, (5), 525-532.

6. Sato, K., Crystallization behaviour of fats and lipids — a review. *Chem. Eng. Sci.* **2001,** 56, (7), 2255-2265.

7. Ivanova, E. A.; Myasoedova, V. A.; Melnichenko, A. A.; Grechko, A. V.; Orekhov, A. N., Small Dense Low-Density Lipoprotein as Biomarker for Atherosclerotic Diseases. *Oxidative Medicine and Cellular Longevity* **2017,** 2017, 10.

8. Kawano, Y.; Cohen, D. E., Mechanisms of hepatic triglyceride accumulation in non-alcoholic fatty liver disease. *Journal of Gastroenterology* **2013,** 48, (4), 434-441.

9. Janoudi, A.; Shamoun, F. E.; Kalavakunta, J. K.; Abela, G. S., Cholesterol crystal induced arterial inflammation and destabilization of atherosclerotic plaque. *European Heart Journal* **2016,** 37, (25), 1959-1967.

10. Clarkson, C. E.; Malkin, T., 139. Alternation in long-chain compounds. Part II. An X-ray and thermal investigation of the triglycerides. *Journal of the Chemical Society (Resumed)* **1934**, (0), 666-671.

11. Cerdeira, M.; Candal, R. J.; Herrera, M. L., Analytical techniques for nucleation studies in lipids: Advantages and disadvantages. *Journal of Food Science* **2004,** 69, (9), R185-R191.

12. Wright, A. J.; Narine, S. S.; Marangoni, A. G., Comparison of experimental techniques used in lipid crystallization studies. *JAOCS, Journal of the American Oil Chemists' Society* **2000,** 77, (12), 1239-1242.

13. Takechi, C.; Kaneko, F., X-ray diffraction and vibrational spectroscopic study of the influence of cis- and trans-unsaturation on the α-phase of triacylglycerols. *J. Phys. Chem. B* **2013,** 117, (29), 8896-8905.

14. Ikeda, E.; Ueno, S.; Miyamoto, R.; Sato, K., Phase behavior of a binary mixture of 1,3-dipalmitoyl-2-oleoyl-sn-glycerol and 1,3-dioleoyl-2-palmitoyl-sn-glycerol in n-dodecane solution. *J. Phys. Chem. B* **2010,** 114, (34), 10961-10969.

15. Harrison, P. D.; Smith, K. W.; Bhaggan, K.; Stapley, A. G. F., Image analysis of palm oil crystallisation as observed by hot stage microscopy. *J. Cryst. Growth* **2016,** 444, 28-38.

16. Ray, J.; MacNaughtan, W.; Chong, P. S.; Vieira, J.; Wolf, B., The Effect of Limonene on the Crystallization of Cocoa Butter. *Journal of the American Oil Chemists' Society* **2012,** 89, (3), 437-445.

17. Toro-Vazquez, J. F.; Rangel-Vargas, E.; Dibildox-Alvarado, E.; Charó-Alonso, M. A., Crystallization of cocoa butter with and without polar lipids evaluated by rheometry, calorimetry and polarized light microscopy. *European Journal of Lipid Science and Technology* **2005,** 107, (9), 641-655.

18. Smith, P. R., The effects of phospholipids on crystallisation and crystal habit in triglycerides. *European Journal of Lipid Science and Technology* **2000,** 102, (2), 122-127.

19. Bresson, S.; Rousseau, D.; Ghosh, S.; El Marssi, M.; Faivre, V., Raman spectroscopy of the polymorphic forms and liquid state of cocoa butter. *European Journal of Lipid Science and Technology* **2011,** 113, (8), 992-1004.

20. Tefelski, D. B.; Jastrzębski, C.; Wierzbicki, M.; Siegoczyński, R. M.; Rostocki, A. J.; Wieja, K.; Kościesza, R., Raman spectroscopy of triolein under high pressures. *High Pressure Research* **2010,** 30, (1), 124-129.

21. Da Silva, E.; Rousseau, D., Molecular order and thermodynamics of the solid-liquid transition in triglycerides viaRaman spectroscopy. *Physical Chemistry Chemical Physics* **2008,** 10, (31), 4606-4613.

22. Bresson, S.; El Marssi, M.; Khelifa, B., Conformational influences of the polymorphic forms on the CO and C–H stretching modes of five saturated monoacid triglycerides studied by Raman spectroscopy at various temperatures. *Vibrational Spectroscopy* **2006,** 40, (2), 263-269.

23. Tandon, P.; Förster, G.; Neubert, R.; Wartewig, S., Phase transitions in oleic acid as studied by X-ray diffraction and FT-Raman spectroscopy. *J. Mol. Struct.* **2000,** 524, (1–3), 201-215.

24. Martini, S.; Herrera, M. L.; Marangoni, A., New technologies to determine solid fat content on-line. *J. Am. Oil Chem. Soc.* **2005,** 82, (5), 313-317.

25. Özilgen, S.; Simoneau, C.; German, J. B.; McCarthy, M. J.; Reid, D. S., Crystallization kinetics of emulsified triglycerides. *Journal of the Science of Food and Agriculture* **1993,** 61, (1), 101-108.

26. Simoneau, C.; McCarthy, M. J.; Reid, D. S.; German, J. B., Measurement of fat crystallization using NMR imaging and spectroscopy. *Trends in Food Science & Technology* **1992,** 3, 208-211.

27. McClements, D. J.; Povey, M. J. W., Comparison of pulsed NMR and ultrasonic velocity techniques for determining solid fat contents. *International Journal of Food Science & Technology* **1988,** 23, (2), 159-170.

28. Norton, I. T.; Lee-Tuffnell, C. D.; Ablett, S.; Bociek, S. M., A calorimetric, NMR and X-ray diffraction study of the melting behavior of tripalmitin and tristearin and their mixing behavior with triolein. *Journal of the American Oil Chemists' Society* **1985,** 62, (8), 1237-1244.

29. Adam-Berret, M.; Boulard, M.; Riaublanc, A.; Mariette, F., Evolution of Fat Crystal Network Microstructure Followed by NMR. *Journal of Agricultural and Food Chemistry* **2011,** 59, (5), 1767-1773.

30. Wang, F.; Liu, Y.; Jin, Q.; Meng, Z.; Wang, X., Characterization of cocoa butter substitutes, milk fat and cocoa butter mixtures. *European Journal of Lipid Science and Technology* **2011,** 113, (9), 1145-1151.

31. Voda, A.; Den Adel, R.; Van Malssen, K.; Van Duynhoven, J., Quantitative Assessment of Triacylglycerol Crystallite Thickness by 1H Spin-Diffusion NMR. *Crystal Growth and Design* **2017,** 17, (4), 1484-1492.

32. Vereecken, J.; Foubert, I.; Smith, K. W.; Dewettinck, K., Effect of SatSatSat and SatOSat on crystallization of model fat blends. *European Journal of Lipid Science and Technology* **2009,** 111, (3), 243-258.

33. Foubert, I.; Fredrick, E.; Vereecken, J.; Sichien, M.; Dewettinck, K., Stop-and-return DSC method to study fat crystallization. *Thermochimica Acta* **2008,** 471, (1–2), 7-13.

34. Kalnin, D.; Lesieur, P.; Artzner, F.; Keller, G.; Ollivon, M., Systematic investigation of lard polymorphism using combined DSC and time-resolved synchrotron X-ray diffraction. *European Journal of Lipid Science and Technology* **2005,** 107, (9), 594-606.

35. Sprunt, J. C.; Jayasooriya, U. A.; Wilson, R. H., A simultaneous FT-Raman-DSC (SRD) study of polymorphism in sn-1,3-distearoyl-2-oleoylglycerol (SOS). *Physical Chemistry Chemical Physics* **2000,** 2, (19), 4299-4305.

36. Arishima, T.; Sagi, N.; Mori, H.; Sato, K., Polymorphism of pos. I. occurrence and polymorphic transformation. *J. Am. Oil Chem. Soc.* **1991,** 68, (10), 710-715.

37. Schlichter Aronhime, J.; Sarig, S.; Garti, N., Reconsideration of polymorphic transformations in cocoa butter using the DSC. *Journal of the American Oil Chemists' Society* **1988,** 65, (7), 1140-1143.

38. Bayés-García, L.; Calvet, T.; Cuevas-Diarte, M. A.; Ueno, S.; Sato, K., Crystallization and transformation of polymorphic forms of trioleoyl glycerol and 1,2-dioleoyl-3-rac-linoleoyl glycerol. *J. Phys. Chem. B* **2013,** 117, (31), 9170-9181.

39. Povey, M. J. W., Applications of ultrasonics in food science - novel control of fat crystallization and structuring. *Curr. Opin. Colloid Interface Sci.* **2017,** 28, 1-6.

40. Winkelmeyer, C. B.; Peyronel, F.; Weiss, J.; Marangoni, A. G., Monitoring Tempered Dark Chocolate Using Ultrasonic Spectrometry. *Food and Bioprocess Technology* **2016,** 9, (10), 1692-1705.

41. Haupler, M.; Peyronel, F.; Neeson, I.; Weiss, J.; Marangoni, A. G., In Situ Ultrasonic Characterization of Cocoa Butter Using a Chirp. *Food and Bioprocess Technology* **2014,** 7, (11), 3186-3196.

42. Wassell, P.; Wiklund, J.; Stading, M.; Bonwick, G.; Smith, C.; Almiron-Roig, E.; Young, N. W. G., Ultrasound Doppler based in-line viscosity and solid fat profile measurement of fat blends. *International Journal of Food Science & Technology* **2010,** 45, (5), 877-883.

43. Hipp, A. K.; Walker, B.; Mazzotti, M.; Morbidelli, M., In-Situ Monitoring of Batch Crystallization by Ultrasound Spectroscopy. *Ind. Eng. Chem. Res.* **2000,** 39, (3), 783-789.

44. McClements, D. J. The use of ultrasonics for characterising fats and emulsions. University of Leeds, 1988.

45. Himawan, C.; MacNaughtan, W.; Farhat, I. A.; Stapley, A. G. F., Polymorphic occurrence and crystallization rates of tristearin/tripalmitin mixtures under non-isothermal conditions. *European Journal of Lipid Science and Technology* **2007,** 109, (1), 49-60.

46. Mykhaylyk, O. O.; Hamley, I. W., The Packing of Triacylglycerols from SAXS Measurements: Application to the Structure of 1,3-Distearoyl-2-oleoyl-sn-glycerol Crystal Phases. *The Journal of Physical Chemistry B* **2004,** 108, (23), 8069-8083.

47. Mykhaylyk, O. O.; Castelletto, V.; Hamley, I. W.; Povey, M. J. W., Structure and transformation of low-temperature phases of 1,3-distearoyl-2-oleoyl glycerol. *European Journal of Lipid Science and Technology* **2004,** 106, (5), 319-324.

48. Dewettinck, K.; Foubert, I.; Basiura, M.; Goderis, B., Phase Behavior of Cocoa Butter in a Two-Step Isothermal Crystallization. *Cryst. Growth Des.* **2004,** 4, (6), 1295-1302.

49. MacMillan, S. D.; Roberts, K. J.; Rossi, A.; Wells, M. A.; Polgreen, M. C.; Smith, I. H., In Situ Small Angle X-ray Scattering (SAXS) Studies of Polymorphism with the Associated Crystallization of Cocoa Butter Fat Using Shearing Conditions. *Cryst. Growth Des.* **2002,** 2, (3), 221-226.

50. Van Langevelde, A.; Peschar, R.; Schenk, H., Structure of β-trimyristin and β-tristearin from high-resolution X-ray powder diffraction data. *Acta Crystallographica Section B* **2001,** 57, (3), 372-377.

51. van Malssen, K.; van Langevelde, A.; Peschar, R.; Schenk, H., Phase behavior and extended phase scheme of static cocoa butter investigated with real-time X-ray powder diffraction. *Journal of the American Oil Chemists' Society* **1999,** 76, (6), 669-676.

52. Ueno, S.; Minato, A.; Yano, J.; Sato, K., Synchrotron radiation X-ray diffraction study of polymorphic crystallization of SOS from liquid phase. *J. Cryst. Growth* **1999,** 198–199, Part 2, (0), 1326-1329.

53. Ueno, S.; Minato, A.; Seto, H.; Amemiya, Y.; Sato, K., Synchrotron Radiation X-ray Diffraction Study of Liquid Crystal Formation and Polymorphic Crystallization of SOS (sn-1,3-Distearoyl-2-oleoyl Glycerol). *The Journal of Physical Chemistry B* **1997,** 101, (35), 6847-6854.

54. van Malssen, K.; Peschar, R.; Schenk, H., Real-time X-ray powder diffraction investigations on cocoa butter. I. temperature-dependent crystallization behavior. *Journal of the American Oil Chemists' Society* **1996,** 73, (10), 1209-1215.

55. Minato, A.; Ueno, S.; Yano, J.; Wang, Z. H.; Seto, H.; Amemiya, Y.; Sato, K., Synchrotron radiation X-ray diffraction study on phase behavior of PPP-POP binary mixtures. *Journal of the American Oil Chemists' Society* **1996,** 73, (11), 1567-1572.

56. Lutton, E. S.; Jackson, F. L.; Quimby, O. T., The polymorphism of the mixed triglycerides of palmitic and stearic acids. *J. Am. Chem. Soc.* **1948,** 70, (7), 2441-2445.

57. Bayés-Garcia, L.; Calvet, T.; Cuevas-Diarte, M. A.; Ueno, S.; Sato, K., Phase behavior of binary mixture systems of saturated-unsaturated mixed-acid triacylglycerols: Effects of glycerol structures and chain-chain interactions. *J. Phys. Chem. B* **2015,** 119, (12), 4417-4427.

58. Verstringe, S.; Dewettinck, K.; Ueno, S.; Sato, K., Triacylglycerol crystal growth: Templating effects of partial glycerols studied with synchrotron radiation microbeam x-ray diffraction. *Crystal Growth and Design* **2014,** 14, (10), 5219-5226.

59. Tascini, A. S.; Noro, M. G.; Chen, R.; Seddon, J. M.; Bresme, F., Understanding the interactions between sebum triglycerides and water: A molecular dynamics simulation study. *Physical Chemistry Chemical Physics* **2018,** 20, (3), 1848-1860.

60. Schmiele, M.; Schindler, T.; Westermann, M.; Steiniger, F.; Radulescu, A.; Kriele, A.; Gilles, R.; Unruh, T., Mesoscopic structures of triglyceride nanosuspensions studied by small-angle X-ray and neutron scattering and computer simulations. *J. Phys. Chem. B* **2014,** 118, (29), 8808-8818.

61. Huang, L.; Lips, A.; Co, C. C., Microemulsification of Triglyceride Sebum and the Role of Interfacial Structure on Bicontinuous Phase Behavior. *Langmuir* **2004,** 20, (9), 3559-3563.

62. Iwahashi, M.; Kasahara, Y., Dynamic molecular movements and aggregation structures of lipids in a liquid state. *Curr. Opin. Colloid Interface Sci.* **2011,** 16, (5), 359-366.

63. Pink, D. A.; Hanna, C. B.; Sandt, C.; MacDonald, A. J.; MacEachern, R.; Corkery, R.; Rousseau, D., Modeling the solid-liquid phase transition in saturated triglycerides. *The Journal of Chemical Physics* **2010,** 132, (5), 054502.

64. Dibildox-Alvarado, E.; Marangoni, A. G.; Toro-Vazquez, J. F., Pre-nucleation structuring of triacylglycerols and its effect on the activation energy of nucleation. *Food Biophysics* **2010,** 5, (3), 218-226.

65. Dibildox-Alvarado, E.; Laredo, T.; Toro-Vazquez, J. F.; Marangoni, A. G., Pre-Nucleation Structuring of TAG Melts Revealed by Fluorescence Polarization Spectroscopy and Molecular Mechanics Simulations. *Journal of the American Oil Chemists' Society* **2010,** 87, (10), 1115-1125.

66. Mykhaylyk, O. O.; Smith, K. W.; Martin, C. M.; Ryan, A. J., Structural models of metastable phases occurring during the crystallization process of saturated/unsaturated triacylglycerols. *J. Appl. Crystallogr.* **2007,** 40, (s1), s297-s302.

67. Larsson, K., On the structure of the liquid state of triglycerides. *J. Am. Oil Chem. Soc.* **1992,** 69, (8), 835-836.

68. Cebula, D.; McClements, D. J.; Povey, M. W.; Smith, P., Neutron diffraction studies of liquid and crystalline trilaurin. *Journal of the American Oil Chemists' Society* **1992,** 69, (2), 130-136.

69. Cebula, D. J.; McClements, D. J.; Povey, M. J. W., Small angle neutron scattering from voids in crystalline trilaurin. *Journal of the American Oil Chemists' Society* **1990,** 67, (2), 76-78.

70. Sato, K.; Bayes-Garcia, L.; Calvet, T.; Angel Cuevas-Diarte, M.; Ueno, S., External factors affecting polymorphic crystallization of lipids. *European Journal of Lipid Science and Technology* **2013,** 115, (11), 1224-1238.

71. Larsson, K., Molecular Arrangement in Glycerides. *Fette, Seifen, Anstrichmittel* **1972,** 74, (3), 136-142.

72. Corkery, R. W.; Rousseau, D.; Smith, P.; Pink, D. A.; Hanna, C. B., A Case for Discotic Liquid Crystals in Molten Triglycerides. *Langmuir* **2007,** 23, (13), 7241-7246.

73. Larsson, K., The Liquid State. In *Lipids-Molecular organisation, physical functions and technical applications*, The Oily Press, L.T.D.: Scotland, 1994; pp 75-80.

74. Seelig, A.; Seelig, J., The dynamic structure of fatty acyl chains in a phospholipid bilayer measured by deuterium magnetic resonance. *Biochemistry* **1974,** 13, (23), 4839-4845.

75. Pabst, G.; Rappolt, M.; Amenitsch, H.; Laggner, P., Structural information from multilamellar liposomes at full hydration: Full q -range fitting with high quality x-ray data. *Physical Review E* **2000,** 62, (3), 4000-4009.

76. Rappolt, M., Bilayer thickness estimations with "poor" diffraction data. *Journal of Applied Physics* **2010,** 107, (8), 084701.

77. Heftberger, P.; Kollmitzer, B.; Heberle, F. A.; Pan, J. J.; Rappolt, M.; Amenitsch, H.; Kucerka, N.; Katsaras, J.; Pabst, G., Global small-angle X-ray scattering data analysis for multilamellar vesicles: the evolution of the scattering density profile model. *J. Appl. Crystallogr.* **2014,** 47, 173-180.

78. Patil-Sen, Y.; Sadeghpour, A.; Rappolt, M.; Kulkarni, C. V., Facile Preparation of Internally Self-assembled Lipid Particles Stabilized by Carbon Nanotubes. *Journal of visualized experiments* **2016**, (108).

79. Pabst, G.; Rappolt, M.; Amenitsch, H.; Laggner, P., Structural information from multilamellar liposomes at full hydration: full q-range fitting with high quality x-ray data. *Physical Review E* **2000,** 62, (3), 4000-4009.

80. Wiener, M. C.; White, S. H., Structure of a fluid dioleoylphosphatidylcholine bilayer determined by joint refinement of x-ray and neutron diffraction data. III. Complete structure. *Biophys.J.* **1992,** 61, 437-447.

81. Brzustowicz, M. R.; Brunger, A. T., X-ray scattering from unilamellar lipid vesicles. *J. Appl. Crystallogr.* **2005,** 38, (1), 126-131.

82. Lin, L. Structure in Liquid Triglycerides. Dalhousie University, Halifax, Nova Scotia, 2014.

83. Rappolt, M.; Laggner, P.; Pabst, G., Structure and elasticity of phospholipid bilayers in the Lα phase: A comparison of phosphatidylcholine and phosphatidylethanolamine membranes. In *Recent Research Developments in Biophysics*, Pandalai, S. G., Ed. Transworld Research Network: Trivandrum, 2004; Vol. 3, Part II, pp 365-394.

84. Nagle, J. F.; Tristram-Nagle, S., Structure of lipid bilayers. *Biochimica et Biophysica Acta (BBA) - Reviews on Biomembranes* **2000,** 1469, (3), 159-195.

85. Drossinos, Y.; Kevrekidis, P. G., Classical nucleation theory revisited. *Physical Review E* **2003,** 67, (2), 026127.

86. Himawan, C.; Starov, V. M.; Stapley, A. G. F., Thermodynamic and kinetic aspects of fat crystallization. *Adv. Colloid Interface Sci.* **2006,** 122, (1-3), 3-33.

87. Povey, M. J. W., Nucleation in food colloids. *The Journal of Chemical Physics* **2016,** 145, (21), 211906.

88. Davis, T.; Dimick, P., Isolation and thermal characterization of high-melting seed crystals formed during cocoa butter solidification. *J. Am. Oil Chem. Soc.* **1989,** 66, (10), 1488-1493.

89. Davis, T.; Dimick, P., Lipid composition of high-melting seed crystals formed during cocoa butter solidification. *J. Am. Oil Chem. Soc.* **1989,** 66, (10), 1494-1498.

90. Floroiu, R. M.; Davis, A. P.; Torrents, A., Cadmium adsorption on aluminum oxide in the presence of polyacrylic acid. *Environ. Sci. Technol.* **2001,** 35, (2), 348-353.

91. Loisel, C.; Keller, G.; Lecq, G.; Bourgaux, C.; Ollivon, M., Phase transitions and polymorphism of cocoa butter. *Journal of the American Oil Chemists' Society* **1998,** 75, (4), 425-439.

92. Hindle, S. A.; Povey, M. J. W.; Smith, K. W., Characterizing cocoa-butter seed crystals by the oil-in-water emulsion crystallization method. *J. Am. Oil Chem. Soc.* **2002,** 79, (10), 993-1002.

93. Takiguchi, H.; Iida, K.; Ueno, S.; Yano, J.; Sato, K., Heterogeneous nucleation of n-alcohol crystals from solution assisted by vapor-deposited thin films of fatty acids. *Journal of Crystal Growth* **1998,** 193, (4), 641-647.

94. Arima, S.; Ueno, S.; Ogawa, A.; Sato, K., Scanning Microbeam Small-Angle X-ray Diffraction Study of Interfacial Heterogeneous Crystallization of Fat Crystals in Oil-in-Water Emulsion Droplets. *Langmuir* **2009,** 25, (17), 9777-9784.

95. Wassell, P.; Okamura, A.; Young, N. W. G.; Bonwick, G.; Smith, C.; Sato, K.; Ueno, S., Synchrotron Radiation Macrobeam and Microbeam X-ray Diffraction Studies of Interfacial Crystallization of Fats in Water-in-Oil Emulsions. *Langmuir* **2012,** 28, (13), 5539-5547.

96. Verstringe, S.; Danthine, S.; Blecker, C.; Depypere, F.; Dewettinck, K., Influence of monopalmitin on the isothermal crystallization mechanism of palm oil. *Food Res. Int.* **2013,** 51, 344.

97. Shimamura, K.; Ueno, S.; Miyamoto, Y.; Sato, K., Effects of polyglycerine fatty acid esters having different fatty acid moieties on crystallization of palm stearin. *Cryst. Growth Des.* **2013,** 13, (11), 4746.

98. Verstringe, S.; Dewettinck, K.; Ueno, S.; Sato, K., Triacylglycerol Crystal Growth: Templating Effects of Partial Glycerols Studied with Synchrotron Radiation Microbeam X-ray Diffraction. *Crystal Growth & Design* **2014,** 14, (10), 5219-5226.

99. Tran, T.; Green, N. L.; Rousseau, D., Spheroidal Fat Crystals: Structure Modification via Use of Emulsifiers. *Crystal Growth & Design* **2015,** 15, (11), 5406-5415.

100. O'Sullivan, C.; Acevedo, N.; Peyronel, F.; Marangoni, A., Fat Nanostructure. In *Edible Nanostructures: a Bottom-up Approach*, Marangoni, A.; Pink, D. A., Eds. Royal Society of Chemistry: Cambridge, 2015; pp 6-40.

101. Acevedo, N. C.; Peyronel, F.; Marangoni, A. G., Nanoscale structure intercrystalline interactions in fat crystal networks. *Current Opinion in Colloid & Interface Science* **2011,** 16, (5), 374-383.

102. Alejandro, G. M.; Sara, E. M., Static Crystallization Behavior of Cocoa Butter and Its Relationship to Network Microstructure. In *Physical Properties of Lipids*, CRC Press: 2002.

103. Chaiseri, S.; Dimick, P. S., Dynamic crystallization of cocoa butter. I. characterization of simple lipids in rapid- and slow-nucleating cocoa butters and their seed crystals. *Journal of the American Oil Chemists' Society* **1995,** 72, (12), 1491-1496.

104. Maggioni, G. M.; Mazzotti, M., Modelling the stochastic behaviour of primary nucleation. *Faraday Discuss.* **2015,** 179, 359-382.